Available online at www.sciencedirect.com
ScienceDirect
Comput. Methods Appl. Mech. Engrg. 360 (2020) 112687
Computer methods in applied mechanics and engineering
www.elsevier.com/locate/cma

Virtual element for the buckling problem of Kirchhoff–Love plates

David Mora[a,b], Iván Velásquez[b,c,*]

[a] GIMNAP, Departamento de Matemática, Universidad del Bío-Bío, Concepción, Chile
[b] $\mathrm{CI^2MA}$, Universidad de Concepción, Concepción, Chile
[c] Departamento de Ingeniería Matemática, Universidad de Concepción, Concepción, Chile

Received 26 February 2019; received in revised form 1 October 2019; accepted 7 October 2019
Available online 29 October 2019

Dedicated to Rodolfo Rodríguez on his 65th birthday

Abstract

In this paper, we develop a virtual element method (VEM) of high order to solve the fourth order plate buckling eigenvalue problem on polygonal meshes. We write a variational formulation based on the Kirchhoff–Love model depending on the transverse displacement of the plate. We propose a C^1 conforming virtual element discretization of arbitrary order $k \geq 2$ and we use the so-called Babuška–Osborn abstract spectral approximation theory to show that the resulting scheme provides a correct approximation of the spectrum and prove optimal order error estimates for the buckling modes (eigenfunctions) and a double order for the buckling coefficients (eigenvalues). Finally, we report some numerical experiments illustrating the behavior of the proposed scheme and confirming our theoretical results on different families of meshes.

MSC: 65N25; 65N30; 74K20; 65N15

Keywords: Virtual element method; Buckling eigenvalue problem; Kirchhoff–Love plates; Error estimates

1. Introduction

In this paper we analyze a conforming C^1 virtual element approximation of an eigenvalue problem arising in Structural Mechanics: the elastic stability of plates, in particular the so-called buckling problem. This problem has attracted much interest since it is frequently encountered in several engineering applications such as car or aircraft design. In particular, we will focus on thin plates which are modeled by the Kirchhoff–Love equations.

The buckling problem for plates can be formulated as a spectral problem of fourth order whose solution is related with the limit of elastic stability of the plate (i.e., eigenvalues-buckling coefficients and eigenfunctions-buckling modes). This problem has been studied with several finite element methods, for instance, conforming and non-conforming discretizations, mixed formulations. We cite as a minimal sample of them [1–8].

The aim of the present paper is to introduce and analyze a virtual element method (VEM) to solve the fourth order plate buckling problem. The VEM has been introduced in [9] and has been applied successfully in a large

* Corresponding author.
E-mail addresses: dmora@ubiobio.cl (D. Mora), ivelasquez@ing-mat.udec.cl (I. Velásquez).

https://doi.org/10.1016/j.cma.2019.112687
0045-7825/

range of problems in fluid and solid mechanics; see for instance [10–27]. Regarding VEM for spectral problems, we mention the following recent works [28–34].

One important advantage of VEM is the possibility of easily implement highly regular discrete spaces to solve fourth order partial differential equations by using conforming subspaces [11,23,35]. It is very well known that the construction of conforming finite elements to H^2 is difficult in general, since they generally involve a large number of degrees of freedom (see [36]). Here, we follow the VEM approach presented in [23,35] to build global discrete spaces of C^1 of arbitrary order that are simple in terms of degrees of freedom and coding aspects to solve an eigenvalue problem modeling the plate buckling problem on general polygonal meshes.

More precisely, we will propose a C^1 Virtual Element Method of arbitrary order $k \geq 2$ to approximate the buckling coefficients and modes of the plate buckling problem on general polygonal meshes. Based on the transverse displacements of the midplane of a thin plate subjected to a symmetric stress tensor field, we propose and analyze a variational formulation in H^2. We characterize the continuous spectrum of the problem through a certain continuous, compact and self-adjoint operator. Then, we exploit the ability of VEM in order to construct highly regular discrete spaces and propose a conforming discretization of the buckling eigenvalue problem in H^2 which is an extension of the discrete virtual space introduced in [11,35]. We construct projection operators in order to write bilinear forms that are fully computable. In particular, to discretize the right hand side of the eigenvalue problem we propose a simple bilinear form which does not need any stabilization. This makes possible to use directly the so-called Babuška–Osborn abstract spectral approximation theory (see [37]) to show that under standard shape regularity assumptions the resulting virtual element scheme provides a correct approximation of the spectrum and prove optimal order error estimates for the eigenfunctions and a double order for the eigenvalues. The proposed VEM method provides an attractive and competitive alternative to solve the fourth order plate buckling eigenvalue problem in terms of its computational cost. For instance, in the lowest order configuration ($k = 2$), the computational cost is almost $3N_v$, where N_v denotes the number of vertices in the polygonal mesh. For $k = 3$, the computational cost is almost $3N_v + N_e$, where N_e denotes the number of edges in the polygonal mesh. Moreover, the resulting eigenvalue problem can be solved with standard eigensolvers (the matrix on the left hand side is symmetric and positive definite). The same happens for conforming finite element methods, but in our case at a lower computational cost. On the other hand, we observe that mixed finite element methods (like Ciarlet–Raviart) lead to a degenerate generalized matrix eigenvalue problem (the matrix resulting is indefinite) which need to be solved with more sofisticated tools.

This paper is structured as follows: In Section 2, we present the variational formulation for the plate buckling eigenvalue problem. We define a solution operator whose spectrum allows us to characterize the spectrum of the buckling problem. In Section 3 we introduce the virtual element discretization of arbitrary degree $k \geq 2$, describe the spectrum of a discrete solution operator and prove some auxiliary results. In Section 4, we prove that the numerical scheme presented in this work provides a correct spectral approximation and establish optimal order error estimates for the eigenvalues and eigenfunctions. Finally, in Section 5 we report some numerical tests that confirm the theoretical analysis developed.

Throughout the article we will use standard notations for Sobolev spaces, norms and seminorms. Moreover, we will denote by C a generic constant independent of the mesh parameter h, which may take different values in different occurrences.

2. Presentation of the continuous spectral problem

Let $\Omega \subseteq \mathbb{R}^2$ be a polygonal bounded domain corresponding to the mean surface of a plate in its reference configuration. The plate is assumed to be homogeneous, isotropic, linearly elastic, and sufficiently thin as to be modeled by Kirchhoff–Love equations. The buckling eigenvalue problem of a clamped plate, which is subjected to a plane stress tensor field $\boldsymbol{\eta} : \Omega \to \mathbb{R}^{2\times 2}$ with $\boldsymbol{\eta} \neq 0$ reads as follows:

$$\begin{cases} \Delta^2 u = -\lambda \operatorname{div}(\boldsymbol{\eta}\nabla u) & \text{in } \Omega, \\ u = \partial_\nu u = 0 & \text{on } \Gamma. \end{cases} \tag{2.1}$$

The unknowns of this eigenvalue problem are the deflection of the plate u (buckling modes) and the eigenvalue λ (scaled buckling coefficients). We have denoted by ∂_ν the normal derivative. To simplify the notation we have taken the Young modulus and the density of the plate, both equal to 1. In addition, the stress tensor field is assumed to satisfy the following equilibrium equations:

$$\begin{aligned} \boldsymbol{\eta}^{\mathrm{t}} &= \boldsymbol{\eta} \quad \text{in } \Omega, \\ \mathbf{div}\, \boldsymbol{\eta} &= 0 \quad \text{in } \Omega. \end{aligned}$$

In the remaining of this section and in Section 3, it is enough to consider $\boldsymbol{\eta} \in L^{\infty}(\Omega)^{2\times 2}$. However, we will assume some additional regularity which will be used in the proof of Theorem 4.4. In addition, we do not need to assume $\boldsymbol{\eta}$ to be positive definite. Let us remark that, in practice, $\boldsymbol{\eta}$ is the stress distribution on the plate subjected to in-plane loads, which does not need to be positive definite [38].

2.1. The continuous formulation

In this section we will present and analyze a variational formulation associated with the spectral problem. We will also introduce the so-called solution operator whose spectra will be related to the solutions of the continuous spectral problem (2.1).

In order to write the variational formulation of the spectral problem, we introduce the following symmetric bilinear forms in $H_0^2(\Omega)$:

$$a(u,v) := \int_{\Omega} D^2u : D^2v, \qquad b(u,v) := \int_{\Omega} (\boldsymbol{\eta}\nabla u)\cdot\nabla v,$$

where ":" denotes the usual scalar product of 2×2-matrices, $D^2v := (\partial_{ij}v)_{1\le i,j\le 2}$ denotes the Hessian matrix of v. It is easy to see that $a(\cdot,\cdot)$ is an inner-product in $H_0^2(\Omega)$.

The variational formulation of the eigenvalue problem (2.1) is given as follows:

Problem 1. Find $(\lambda,u)\in\mathbb{R}\times H_0^2(\Omega)$, $u\neq 0$, such that

$$a(u,v) = \lambda b(u,v) \qquad \forall v\in H_0^2(\Omega). \tag{2.2}$$

The following result establishes that the bilinear form $a(\cdot,\cdot)$ is elliptic in $H_0^2(\Omega)$.

Lemma 2.1. *There exists a constant $\alpha_0>0$, depending on Ω, such that*

$$a(v,v) \ge \alpha_0 \|v\|_{2,\Omega}^2 \qquad \forall v\in H_0^2(\Omega).$$

Proof. The result follows immediately from the fact that $\|D^2v\|_{0,\Omega}$ is a norm on $H_0^2(\Omega)$, equivalent with the usual norm. $\square$

Remark 2.1. We have that $\lambda\neq 0$ in problem (2.2). Moreover, it is easy to prove, using the symmetry of $\boldsymbol{\eta}$, that all the eigenvalues are real (not necessarily positive). We also have that $b(u,u)\neq 0$.

Next, in order to analyze the variational eigenvalue problem (2.2), we introduce the following solution operator:

$$\begin{aligned} T :\ & H_0^2(\Omega) \longrightarrow H_0^2(\Omega),\\ & f \longmapsto Tf := w, \end{aligned}$$

where $w\in H_0^2(\Omega)$ is the unique solution (as a consequence of Lemma 2.1) of the following source problem:

$$a(w,v) = b(f,v) \qquad \forall v\in H_0^2(\Omega). \tag{2.3}$$

We have that the linear operator T is well defined and bounded. Notice that $(\lambda,u)\in\mathbb{R}\times H_0^2(\Omega)$ solves problem (2.2) if and only if $Tu=\mu u$ with $\mu\neq 0$ and $u\neq 0$, in which case $\mu := \frac{1}{\lambda}$. In addition, using the symmetry of $\boldsymbol{\eta}$, we can deduce that T is self-adjoint with respect to the inner product $a(\cdot,\cdot)$ in $H_0^2(\Omega)$. Indeed, given $f,g\in H_0^2(\Omega)$,

$$a(Tf,g) = b(f,g) = b(g,f) = a(Tg,f) = a(f,Tg).$$

On the other hand, the following is an additional regularity result for the solution of problem (2.3) and consequently, for the eigenfunctions of T.

Lemma 2.2. *There exists $s_\Omega > 1/2$ such that the following results hold:*

(i) For all $f \in H^1(\Omega)$, there exists a positive constant $C > 0$ such that any solution w of the source problem (2.3) satisfies $w \in H^{2+\tilde{s}}(\Omega)$ with $\tilde{s} := \min\{s_\Omega, 1\}$ and

$$\|w\|_{2+\tilde{s},\Omega} \leq C\|f\|_{1,\Omega}.$$

(ii) If (λ, u) is an eigenpair of the spectral problem (2.2), there exist $s > 1/2$ and a positive constant C depending only on Ω such that $u \in H^{2+s}(\Omega)$ and

$$\|u\|_{2+s,\Omega} \leq C\|u\|_{2,\Omega}.$$

Proof. The proof follows from the classical regularity result for the biharmonic problem with its right-hand side in $L^2(\Omega)$ (cf. [39]). □

Therefore, because of the compact inclusion $H^{2+s}(\Omega) \hookrightarrow H_0^2(\Omega)$, T is a compact operator. Thus, we finish this section with the following spectral characterization result.

Lemma 2.3. *The spectrum of T satisfies $\mathrm{sp}(T) = \{0\} \cup \{\mu_k\}_{k\in\mathbb{N}}$, where $\{\mu_k\}_{k\in\mathbb{N}}$ is a sequence of real eigenvalues which converges to 0. The multiplicity of each eigenvalue is finite.*

Remark 2.2. The buckling eigenvalue problem (2.1) can be analyzed with other types of boundary conditions. For instance, if the plate is considered to be clamped on part Γ_c, simply supported on part Γ_s and free on Γ_f:

$$\Gamma := \Gamma_c \cup \Gamma_s \cup \Gamma_f.$$

We assume that Γ_c, Γ_s and Γ_f are finite sums of connected components and that Γ_c, Γ_s are given such that rigid-body motions are avoided. Thus, in this case, the deflection of the plate, belong to the Sobolev space:

$$W := \{w \in H^2(\Omega) : w = 0 \text{ on } \Gamma_c \cup \Gamma_s, \quad \partial_\nu w = 0 \text{ on } \Gamma_c\}.$$

In this case, the theoretical and numerical analysis presented in the next sections can be developed with the same arguments as those applied for a clamped plate. We mention that numerical verification of test cases involving other types of boundary conditions will be addressed in Section 5, where we observe optimal convergence.

3. Spectral approximation

In this section, we will write a VEM discretization of the spectral problem (2.2). With this aim, we start with the mesh construction and the assumptions considered to introduce the discrete virtual element spaces.

Let $\{\mathcal{T}_h\}_h$ be a sequence of decompositions of Ω into polygons K we will denote by h_K the diameter of the element K and h the maximum of the diameters of all the elements of the mesh, i.e., $h := \max_{K\in\mathcal{T}_h} h_K$. In what follows, we denote by N_K the number of vertices of K, by e a generic edge of $\{\mathcal{T}_h\}_h$ and for all $e \in \partial K$, we define a unit normal vector ν_K^e that points outside of K.

In addition, we will make the following assumptions as in [9,28]: there exists a positive real number $C_\mathcal{T}$ such that, for every h and every $K \in \mathcal{T}_h$,

A1: $K \in \mathcal{T}_h$ is star-shaped with respect to every point of a ball of radius $C_\mathcal{T} h_K$;
A2: the ratio between the shortest edge and the diameter h_K of K is larger than $C_\mathcal{T}$.

In order to introduce the discretization, for every integer $k \geq 2$ and for every polygon K, we define the following finite dimensional space:

$$\widetilde{V}_h^K := \Big\{v_h \in H^2(K) : \Delta^2 v_h \in \mathbb{P}_{k-2}(K), v_h|_{\partial K} \in C^0(\partial K), v_h|_e \in \mathbb{P}_r(e)\ \forall e \in \partial K,$$
$$\nabla v_h|_{\partial K} \in C^0(\partial K)^2, \partial_{\nu_K^e} v_h|_e \in \mathbb{P}_s(e)\ \forall e \in \partial K\Big\},$$

where $r := \max\{3, k\}$ and $s := k - 1$.

This space has been recently considered in [23] to obtain optimal error estimates for fourth order PDEs and it can be seen as an extension of the C^1 virtual space introduced in [35] to solve the bending problem of thin plates.

Here, we will consider the same space together with an enhancement technique (cf. [40]) to build a computable right hand of the buckling eigenvalue problem.

It is easy to see that any $v_h \in \widetilde{V}_h^K$ satisfies the following conditions:

- the trace (and the trace of the gradient) on the boundary of K is continuous;
- $\mathbb{P}_k(K) \subseteq \widetilde{V}_h^K$.

In $\widetilde{V}_h^K$ we define the following five sets of linear operators. For all $v_h \in \widetilde{V}_h^K$:

$\mathbf{D_1}$: evaluation of v_h at the N_K vertices of K;
$\mathbf{D_2}$: evaluation of ∇v_h at the N_K vertices of K;
$\mathbf{D_3}$: For $r > 3$, the moments $\int_e q(\xi) v_h(\xi) d\xi \quad \forall q \in \mathbb{P}_{r-4}(e), \quad \forall$ edge e;
$\mathbf{D_4}$: For $s > 1$, the moments $\int_e q(\xi) \partial_{\nu_K^e} v_h(\xi) d\xi \quad \forall q \in \mathbb{P}_{s-2}(e), \quad \forall$ edge e;
$\mathbf{D_5}$: For $k \geq 4$, the moments $\int_K q(\boldsymbol{x}) v_h(\boldsymbol{x}) d\boldsymbol{x} \quad \forall q \in \mathbb{P}_{k-4}(K), \quad \forall$ polygon K.

In order to construct the discrete scheme, we need some preliminary definitions. First, we note that bilinear form $a(\cdot,\cdot)$, introduced in the previous section, can be split as follows:

$$a(u,v) = \sum_{K\in\mathcal{T}_h} a_K(u,v), \qquad u, v \in H_0^2(\Omega),$$

with

$$a_K(u,v) := \int_K D^2 u : D^2 v, \qquad u, v \in H^2(K).$$

Now, we define the projector $\Pi_K^{k,D} : H^2(K) \to \mathbb{P}_k(K) \subseteq \widetilde{V}_h^K$ as the solution of the following local problems (in each element K):

$$a_K\big(\Pi_K^{k,D} v, q\big) = a_K(v,q) \qquad \forall q \in \mathbb{P}_k(K) \quad \forall v \in H^2(K), \tag{3.1a}$$
$$\widehat{\Pi_K^{k,D} v} = \widehat{v}, \quad \widehat{\nabla \Pi_K^{k,D} v} = \widehat{\nabla v}, \tag{3.1b}$$

where $\widehat{v}$ is defined as follows:

$$\widehat{v} := \frac{1}{N_K} \sum_{i=1}^{N_K} v(\mathrm{v}_i) \qquad \forall v \in C^0(\partial K)$$

and v_i, $1 \leq i \leq N_K$, are the vertices of K.

We observe that bilinear form $a_K(\cdot,\cdot)$ has a non-trivial kernel given by $\mathbb{P}_1(K)$. Hence, the role of condition (3.1b) is to select an element of the kernel of the operator.

It is easy to see that operator $\Pi_K^{k,D}$ is well defined on $\widetilde{V}_h^K$. Moreover, the following result states that for all $v \in \widetilde{V}_h^K$ the polynomial $\Pi_K^{k,D} v$ can be computed using the output values of the sets $\mathbf{D_1}$–$\mathbf{D_5}$.

Lemma 3.1. *The operator $\Pi_K^{k,D} : \widetilde{V}_h^K \to \mathbb{P}_k(K)$ is explicitly computable for every $v \in \widetilde{V}_h^K$, using only the information of the linear operators in* $\mathbf{D_1}$–$\mathbf{D_5}$.

Proof. For all $v_h \in \widetilde{V}_h^K$ we integrate twice by parts on the right-hand side of (3.1a). We obtain

$$\begin{aligned} a(v_h, q) &= \int_K D^2 v_h : D^2 q \\ &= \int_K \Delta^2 q v_h - \int_{\partial K} \mathbf{div}(D^2 q) \cdot \nu_K v_h + \int_{\partial K} D^2 q \nu_K \cdot \nabla v_h. \end{aligned} \tag{3.2}$$

It is easy to see that since $\Delta^2 q \in \mathbb{P}_{k-4}(K)$ hence the first integral on the right-hand side of (3.2) is computable using the output values of the set $\mathbf{D_5}$. We also note that the boundary integrals of (3.2) only depend on the boundary values of v_h and ∇v_h, so they are computable using the output values of the sets $\mathbf{D_1}$–$\mathbf{D_4}$. On the other hand, the kernel part of $\Pi_K^{k,D}$ (cf. (3.1b)) is computable using the output values of the sets $\mathbf{D_1}$–$\mathbf{D_2}$. $\square$

We introduce our local virtual space:

$$V_h^K := \left\{ v_h \in \widetilde{V}_h^K : \int_K (\Pi_K^{k,D} v_h) q = \int_K v_h q \qquad \forall q \in \mathbb{P}_{k-3}^*(K) \cup \mathbb{P}_{k-2}^*(K) \right\},$$

where $\mathbb{P}_\ell^*(K)$ denotes homogeneous polynomials of degree ℓ with the convention that $\mathbb{P}_{-1}^*(K) = \{0\}$.

Note that $V_h^K \subseteq \widetilde{V}_h^K$. Thus, the linear operator $\Pi_K^{k,D}$ is well defined on V_h^K and computable only using the output values of the sets $\mathbf{D_1}$–$\mathbf{D_5}$. We also have that $\mathbb{P}_k(K) \subseteq V_h^K$. This will guarantee the good approximation properties of the space.

Moreover, it has been established in [23] that the set of linear operators $\mathbf{D_1}$–$\mathbf{D_5}$ constitutes a set of degrees of freedom for V_h^K.

Now, we consider the $L^2(K)$ orthogonal projector onto $\mathbb{P}_{k-2}(K)$ as follows: we define $\Pi_K^{k-2} : L^2(K) \to \mathbb{P}_{k-2}(K)$ for each $v \in L^2(K)$ by

$$\int_K (\Pi_K^{k-2} v) q = \int_K v q \qquad \forall q \in \mathbb{P}_{k-2}(K). \tag{3.3}$$

Next, due to the particular property appearing in definition of the space V_h^K, it can be seen that the right hand side in (3.3) is computable using $\Pi_K^{k,D} v$, and the degrees of freedom given by $\mathbf{D_5}$ and thus $\Pi_K^{k-2} v$ depends only on the values of the degrees of freedom given by $\mathbf{D_1}$–$\mathbf{D_5}$ when $v \in V_h^K$.

In order to discretize the right hand side of the buckling eigenvalue problem, we will consider the following projector onto $\mathbb{P}_{k-1}(K)^2$: we define $\boldsymbol{\Pi}_K^{k-1} : H^1(K) \to \mathbb{P}_{k-1}(K)^2$ for each $v \in H^1(K)$ by

$$\int_K (\boldsymbol{\Pi}_K^{k-1} \nabla v) \cdot \mathbf{q} = \int_K \nabla v \cdot \mathbf{q} \quad \forall \mathbf{q} \in \mathbb{P}_{k-1}(K)^2.$$

In addition, we observe that the for any $v_h \in V_h^K$, the vector function $\boldsymbol{\Pi}_K^{k-1} \nabla v_h$ can be explicitly computed from the degrees of freedom $\mathbf{D_1}$–$\mathbf{D_5}$. In fact, in order to compute $\boldsymbol{\Pi}_K^{k-1} \nabla v_h$, for all $K \in \mathcal{T}_h$ we must be able to calculate the following:

$$\int_K \nabla v_h \cdot \mathbf{q} \qquad \forall \mathbf{q} \in \mathbb{P}_{k-1}(K)^2.$$

From an integration by parts, we have

$$\begin{aligned} \int_K \nabla v_h \cdot \mathbf{q} &= -\int_K v_h \operatorname{div} \mathbf{q} + \int_{\partial K} v_h (\mathbf{q} \cdot \nu_K) \qquad \forall \mathbf{q} \in \mathbb{P}_{k-1}(K)^2, \\ &= -\int_K \Pi_K^{k-2} v_h \operatorname{div} \mathbf{q} + \int_{\partial K} v_h (\mathbf{q} \cdot \nu_K) \qquad \forall \mathbf{q} \in \mathbb{P}_{k-1}(K)^2. \end{aligned}$$

The first term on the right-hand side above depends only on the $\Pi_K^{k-2} v_h$ and this depends on the values of the degrees of freedom $\mathbf{D_1}$–$\mathbf{D_5}$ (cf. (3.3)). The second term can also be computed since $\mathbf{q}$ is a polynomial of degree $k-1$ on each edge and therefore is uniquely determined by the values of $\mathbf{D_1}$–$\mathbf{D_5}$.

Now, we are ready to define our global virtual space to solve the plate buckling eigenvalue problem, this is defined as follows:

$$V_h := \left\{ v_h \in H_0^2(\Omega) : v_h|_K \in V_h^K \right\}. \tag{3.4}$$

In what follows, we discuss the construction of the discrete version of the local forms. With this aim, we consider $s_K^D(\cdot,\cdot)$ any symmetric positive definite and computable bilinear form to be chosen as to satisfy:

$$c_0 a_K(v_h, v_h) \le s_K^D(v_h, v_h) \le c_1 a_K(v_h, v_h) \quad \forall v_h \in V_h^K \quad \text{with} \qquad \Pi_K^{k,D} v_h = 0. \tag{3.5}$$

Then, we set

$$a_h(u_h, v_h) := \sum_{K \in \mathcal{T}_h} a_{h,K}(u_h, v_h), \qquad u_h, v_h \in V_h,$$

$$b_h(u_h, v_h) := \sum_{K \in \mathcal{T}_h} b_{h,K}(u_h, v_h), \qquad u_h, v_h \in V_h,$$

where, $a_{h,K}(\cdot,\cdot)$ is the local bilinear form on $V_h^K \times V_h^K$ defined by

$$a_{h,K}(u_h, v_h) := a_K\big(\Pi_K^{k,D} u_h, \Pi_K^{k,D} v_h\big) + s_K^D\big(u_h - \Pi_K^{k,D} u_h, v_h - \Pi_K^{k,D} v_h\big). \tag{3.6}$$

Notice that the bilinear form $s_K^D(\cdot,\cdot)$ has to be actually computable for $u_h, v_h \in V_h^K$.

On the other hand, we will propose on each element K the following local, computable and nonstabilized approximation for the bilinear form $b(\cdot,\cdot)$ (cf. Section 2.1):

$$b_{h,K}(u_h, v_h) := \int_K \boldsymbol{\eta} \boldsymbol{\Pi}_K^{k-1} \nabla u_h \cdot \boldsymbol{\Pi}_K^{k-1} \nabla v_h. \tag{3.7}$$

Proposition 3.1. *The local bilinear form $a_{h,K}(\cdot,\cdot)$ on each element K satisfy*

- *Consistency: for all $h > 0$ and for all $K \in \mathcal{T}_h$, we have that*

$$a_{h,K}(p, v_h) = a_K(p, v_h) \qquad \forall p \in \mathbb{P}_k(K), \quad \forall v_h \in V_h^K, \tag{3.8}$$

- *Stability and boundedness: There exist two positive constants α_1, α_2, independent of K, such that:*

$$\alpha_1 a_K(v_h, v_h) \le a_{h,K}(v_h, v_h) \le \alpha_2 a_K(v_h, v_h) \qquad \forall v_h \in V_h^K. \tag{3.9}$$

3.1. The discrete eigenvalue problem

Now, we are in a position to write the virtual element discretization of Problem 1 as follows.

Problem 2. Find $(\lambda_h, u_h) \in \mathbb{R} \times V_h$, $u_h \neq 0$, such that

$$a_h(u_h, v_h) = \lambda_h b_h(u_h, v_h) \qquad \forall v_h \in V_h. \tag{3.10}$$

We observe that by virtue of (3.9), the bilinear form $a_h(\cdot,\cdot)$ is bounded. Moreover, as shown in the following lemma, it is also uniformly elliptic.

Lemma 3.2. *There exists a constant $\alpha > 0$, independent of h, such that*

$$a_h(v_h, v_h) \ge \alpha \, \|v_h\|_{2,\Omega}^2 \qquad \forall v_h \in V_h.$$

Proof. Thanks to (3.9) and Lemma 2.1, it is easy to check that the above inequality holds with $\alpha := \alpha_0 \min\{\alpha_1, 1\}$. $\square$

In order to analyze the discrete problem, we introduce the solution operator associated to Problem 2 as follows:

$$T_h : H_0^2(\Omega) \longrightarrow H_0^2(\Omega),$$
$$f \longmapsto T_h f := w_h,$$

with w_h the unique solution of the following source problem

$$a_h(w_h, v_h) = b_h(f, v_h) \qquad \forall v_h \in V_h. \tag{3.11}$$

Note that the ellipticity of $a_h(\cdot,\cdot)$ established in Lemma 3.2, the boundedness of the right hand side (cf. (3.7)) and Lax–Milgram Lemma guarantee that T_h is well defined. Moreover, as in the continuous case, $(\lambda_h, u_h) \in \mathbb{R} \times V_h$ solves problem (3.10) if and only if $T_h u_h = \mu_h u_h$ with $\mu_h \neq 0$ and $u_h \neq 0$, in which case $\mu_h := \frac{1}{\lambda_h}$.

Remark 3.1. The same arguments leading to Remark 2.1 allow us to show that any solution of (3.10) satisfies $\lambda_h \neq 0$. Moreover, $b_h(u_h, u_h) \neq 0$ also holds true.

Moreover from the definition of $a_h(\cdot,\cdot)$ and $b_h(\cdot,\cdot)$ we can check that T_h is self-adjoint with respect to inner product $a_h(\cdot,\cdot)$. Therefore, we can describe the spectrum of the solution operator T_h.

Now, we are in position to write the following characterization of the spectrum of the solution operator.

Theorem 3.1. *The spectrum of T_h consists of $M_h := \dim(V_h)$ eigenvalues, repeated according to their respective multiplicities. The spectrum decomposes as follows: $\mathrm{sp}(T_h) = \{0\} \cup \{\mu_h\}_{k=1}^{\kappa}$, where $\kappa = M_h - \dim Z_h$ with $Z_h := \{u_h \in V_h : b_h(u_h, v_h) = 0 \quad \forall v_h \in V_h\}$. The eigenvalues μ_h are all real and non-zero.*

4. Convergence and error estimates

In this section we will establish convergence and error estimates of the proposed VEM discretization. With this aim, we will prove that T_h provides a correct spectral approximation of T using the classical theory for compact operators (see [37]).

We start with the following approximation result, on star-shaped polygons, which is derived by interpolation between Sobolev spaces (see for instance [41, Theorem I.1.4] from the analogous result for integer values of s). We mention that this result has been stated in [9, Proposition 4.2] for integer values and follows from the classical Scott–Dupont theory (see [42] and [11, Proposition 3.1]):

Proposition 4.1. *There exists a constant $C > 0$, such that for every $v \in H^{\delta}(K)$ there exists $v_\pi \in \mathbb{P}_k(K)$, $k \geq 0$ such that*

$$|v - v_\pi|_{\ell,K} \leq C h_K^{\delta-\ell} |v|_{\delta,K} \quad 0 \leq \delta \leq k+1, \ell = 0, \dots, [\delta],$$

with $[\delta]$ denoting largest integer equal to or smaller than $\delta \in \mathbb{R}$.

In what follows, we write several auxiliary results which will be useful in the forthcoming analysis. First, we write standard error estimations for the projector $\boldsymbol{\Pi}_K^{k-1}$.

Lemma 4.1. *There exists $C > 0$ independent of h such that for all $\mathbf{v} \in H^{\delta}(K)^2$*

$$\|\mathbf{v} - \boldsymbol{\Pi}_K^{k-1}\mathbf{v}\|_{0,K} \leq C h_K^{\delta} |\mathbf{v}|_{\delta,K} \quad 0 \leq \delta \leq k.$$

Now, we present an interpolation result in the virtual space V_h (see [11,43]).

Proposition 4.2. *Assume **A1–A2** are satisfied, then for all $v \in H^s(\Omega)$ there exist $v_I \in V_h$ and $C > 0$ independent of h such that*

$$\|v - v_I\|_{l,K} \leq C h_K^{s-l} |v|_{s,K}, \quad l = 0, 1, 2, \quad 2 \leq s \leq k+1.$$

Now, in order to prove the convergence of our method, we introduce the following broken H^s-seminorm ($s = 1, 2$):

$$|v|_{s,h} := \Big(\sum_{K \in \mathcal{T}_h} |v|_{s,K}^2 \Big)^{1/2},$$

which is well defined for every $v \in L^2(\Omega)$ such that $v|_K \in H^s(K)$ for all polygon $K \in \mathcal{T}_h$.

Now, with these definitions we have the following results.

Lemma 4.2. *There exists $C > 0$ such that, for all $f \in H_0^2(\Omega)$, if $w = Tf$ and $w_h = T_h f$, then*

$$\|(T - T_h) f\|_{2,\Omega} = \|w - w_h\|_{2,\Omega} \leq C\Big(h\|f\|_{2,\Omega} + \|w - w_I\|_{2,\Omega} + |w - w_\pi|_{2,h}\Big),$$

for all $w_I \in V_h$ and for all $w_\pi \in L^2(\Omega)$ such that $w_\pi|_K \in \mathbb{P}_k(K) \quad \forall K \in \mathcal{T}_h$.

Proof. Let $f \in H_0^2(\Omega)$, and $w = Tf$ and $w_h = T_h f$. For $w_I \in V_h$, we set $v_h := w_h - w_I$. Thus

$$\|(T - T_h)f\|_{2,\Omega} \leq \|w - w_I\|_{2,\Omega} + \|v_h\|_{2,\Omega}. \tag{4.1}$$

Now, thanks to Lemma 3.2, the definition of $a_{h,K}(\cdot,\cdot)$ and those of T and T_h, we have

$$
\begin{aligned}
\alpha\|v_h\|_{2,\Omega}^2 &\leq a_h(v_h,v_h) = a_h(w_h,v_h) - a_h(w_I,v_h) = a_h(w_h,v_h) - \sum_{K\in\mathcal{T}_h} a_{h,K}(w_I,v_h)\\
&= a_h(w_h,v_h) - \sum_{K\in\mathcal{T}_h}\Big\{a_{h,K}(w_I-w_\pi,v_h) + a_{h,K}(w_\pi,v_h)\Big\}\\
&= a_h(w_h,v_h) - \sum_{K\in\mathcal{T}_h}\Big\{a_{h,K}(w_I-w_\pi,v_h) + a_K(w_\pi-w,v_h) + a_K(w,v_h)\Big\}\\
&= a_h(w_h,v_h) - a(w,v_h) - \sum_{K\in\mathcal{T}_h}\Big\{a_{h,K}(w_I-w_\pi,v_h) + a_K(w_\pi-w,v_h)\Big\}. \qquad (4.2)
\end{aligned}
$$

We bound each term on the right hand side of (4.2). The first term can be estimated as follows

$$
\begin{aligned}
&a_h(w_h,v_h) - a(w,v_h) = b_h(f,v_h) - b(f,v_h)\\
&= \sum_{K\in\mathcal{T}_h}\left\{\int_K \{\boldsymbol{\eta}\boldsymbol{\Pi}_K^{k-1}\nabla f\cdot\boldsymbol{\Pi}_K^{k-1}\nabla v_h - \boldsymbol{\eta}\nabla f\cdot\nabla v_h\}\right\}\\
&= \sum_{K\in\mathcal{T}_h}\left\{\int_K \{\boldsymbol{\eta}\boldsymbol{\Pi}_K^{k-1}\nabla f\cdot\boldsymbol{\Pi}_K^{k-1}\nabla v_h - \boldsymbol{\eta}\nabla f\cdot\boldsymbol{\Pi}_K^{k-1}\nabla v_h + \boldsymbol{\eta}\nabla f\cdot\boldsymbol{\Pi}_K^{k-1}\nabla v_h - \boldsymbol{\eta}\nabla f\cdot\nabla v_h\}\right\}\\
&= \sum_{K\in\mathcal{T}_h}\left\{\int_K \{\boldsymbol{\eta}\left(\boldsymbol{\Pi}_K^{k-1}\nabla f - \nabla f\right)\cdot\boldsymbol{\Pi}_K^{k-1}\nabla v_h + \boldsymbol{\eta}\nabla f\cdot\left(\boldsymbol{\Pi}_K^{k-1}\nabla v_h - \nabla v_h\right)\}\right\}\\
&\leq \sum_{K\in\mathcal{T}_h} C\left\{\|\boldsymbol{\Pi}_K^{k-1}\nabla f - \nabla f\|_{0,K}\|\boldsymbol{\Pi}_K^{k-1}\nabla v_h\|_{0,K} + \|\nabla f\|_{0,K}\|\boldsymbol{\Pi}_K^{k-1}\nabla v_h - \nabla v_h\|_{0,K}\right\}\\
&\leq Ch\|f\|_{2,\Omega}\|v_h\|_{2,\Omega},
\end{aligned}
$$

where we have used Lemma 4.1 in the last inequality. Notice that the constant $C>0$ depends on $\|\boldsymbol{\eta}\|_\infty$.

Next, using the stability of $a_{h,K}(\cdot,\cdot)$, the Cauchy–Schwarz and triangular inequalities in the second term on the right hand side of (4.2), we have

$$
\alpha\,\|v_h\|_{2,\Omega}^2 \leq C\Big(h\|f\|_{2,\Omega} + \|w-w_I\|_{2,\Omega} + |w-w_\pi|_{2,h}\Big)\|v_h\|_{2,\Omega}.
$$

Thus, the result follows from the previous bounds together with (4.2). $\square$

Now we are in a position to prove that the operator T_h converges in norm to T.

Theorem 4.1. *For all $f\in H_0^2(\Omega)$, there exist $\tilde{s}\in(\frac{1}{2},1]$ and $C>0$ independent of h such that*

$$
\|(T-T_h)f\|_{2,\Omega} \leq Ch^{\tilde{s}}\|f\|_{2,\Omega}.
$$

Proof. The proof is obtained from Lemma 4.2 and Propositions 4.1 and 4.2 and Lemma 2.2. $\square$

Next, we will use the classical theory for compact operators (see [37] for instance) in order to prove convergence and error estimates for eigenfunctions and eigenvalues. Indeed, an immediate consequence of Theorem 4.1 is that isolated parts of $\mathrm{sp}(T)$ are approximated by isolated parts of $\mathrm{sp}(T_h)$. It means that if μ is a nonzero eigenvalue of T with algebraic multiplicity m, hence there exist m eigenvalues $\mu_h^{(1)},\ldots,\mu_h^{(m)}$ of T_h (repeated according to their respective multiplicities) that will converge to μ as h goes to zero.

Now, let us denote by $\mathcal{E}$ and $\mathcal{E}_h$ the eigenspace associated to the eigenvalue μ and the spanned of the eigenspaces associated to $\mu_h^{(1)},\ldots,\mu_h^{(m)}$, respectively.

We also recall the definition of the *gap* $\widehat{\delta}$ between two closed subspaces $\mathcal{X}$ and $\mathcal{Y}$ of a Hilbert space $\mathcal{V}$:

$$
\widehat{\delta}(\mathcal{X},\mathcal{Y}) := \max\left\{\delta(\mathcal{X},\mathcal{Y}),\delta(\mathcal{Y},\mathcal{X})\right\},
$$

where

$$
\delta(\mathcal{X},\mathcal{Y}) := \sup_{\mathbf{x}\in\mathcal{X}:\ \|x\|_{\mathcal{V}}=1}\delta(x,\mathcal{Y}), \quad \text{with } \delta(x,\mathcal{Y}) := \inf_{y\in\mathcal{Y}}\|x-y\|_{\mathcal{V}}.
$$

We also define

$$\gamma_h := \sup_{f\in\mathcal{E}:\|f\|_{2,\Omega}=1} \|(T-T_h)f\|_{2,\Omega}.$$

The following error estimates for the approximation of eigenvalues and eigenfunctions hold true which is obtained from Theorems 7.1 and 7.3 from [37].

Theorem 4.2. *There exists a strictly positive constant C such that*

$$\widehat{\delta}(\mathcal{E},\mathcal{E}_h) \leq C\gamma_h,$$
$$\left|\mu-\mu_h^{(j)}\right| \leq C\gamma_h \qquad \forall j=1,\dots,m.$$

Moreover, employing the additional regularity of the eigenfunctions, we immediately obtain the following bound.

Theorem 4.3. *There exist $s>1/2$ and $C>0$ independent of h such that*

$$\|(T-T_h)f\|_{2,\Omega} \leq Ch^{\min\{s,k-1\}}\|f\|_{2,\Omega} \qquad \forall f\in\mathcal{E}, \tag{4.3}$$

and as a consequence,

$$\gamma_h \leq Ch^{\min\{s,k-1\}}. \tag{4.4}$$

Proof. The inequality (4.3) can be obtained by repeating the same steps like in the proof of Theorem 4.1 and Lemma 2.2. Estimate (4.4) follows from the definition of γ_h and (4.3). $\square$

Remark 4.1. The error estimate obtained for the eigenpair (μ,u) of T in Theorem 4.2 implies similar estimates for the eigenpair $(\lambda := 1/\mu, u)$ of Problem 1 by means of the discrete eigenvalues $\lambda_h^{(j)} = 1/\mu_h^{(j)}$, $1\leq j\leq m$.

Now, in what follows we will prove a double order of convergence for the eigenvalue approximation. To prove this, we are going to assume that $\boldsymbol{\eta}$ is a smooth enough tensor.

Theorem 4.4. *There exists a positive constant independent of h such that*

$$|\lambda-\lambda_h^{(j)}| \leq Ch^{2\min\{s,k-1\}} \qquad \forall j=1,\dots,m.$$

Proof. Let $u_h\in\mathcal{E}_h$ be an eigenfunction corresponding to one of the eigenvalues $\lambda_h^{(j)}$, $j=1,\dots,m$, with $\|u_h\|_{2,\Omega}=1$. From Theorem 4.2, we have that there exists $u\in\mathcal{E}$ satisfying

$$\|u-u_h\|_{2,\Omega} \leq C\gamma_h. \tag{4.5}$$

It is easy to see that from the symmetry of the bilinear forms in the continuous and discrete spectral problems (cf. Problems 1 and 2), we have

$$\begin{aligned} a(u-u_h,u-u_h)-\lambda b(u-u_h,u-u_h) &= a(u_h,u_h)-\lambda b(u_h,u_h)\\ &= a(u_h,u_h)-a_h(u_h,u_h)+\lambda_h^{(j)}b_h(u_h,u_h)-\lambda b(u_h,u_h)\\ &= a(u_h,u_h)-a_h(u_h,u_h)+(\lambda_h^{(j)}-\lambda)b_h(u_h,u_h)+\lambda[b_h(u_h,u_h)-b(u_h,u_h)], \end{aligned}$$

and therefore we have the following identity

$$\begin{aligned} (\lambda_h^{(i)}-\lambda)b_h(u_h,u_h) &= a(u-u_h,u-u_h)-\lambda b(u-u_h,u-u_h)\\ &\quad +(a_h(u_h,u_h)-a(u_h,u_h))+\lambda\left[b(u_h,u_h)-b_h(u_h,u_h)\right]. \end{aligned} \tag{4.6}$$

Now, we will bound each term on the right hand side of (4.6). For the first and second term we deduce

$$a(u-u_h,u-u_h) = |u-u_h|_{2,\Omega}^2 \leq C\gamma_h^2,$$

and

$$b(u-u_h,u-u_h) = \int_\Omega \boldsymbol{\eta}\boldsymbol{\Pi}_K^{k-1}\nabla(u-u_h)\cdot\boldsymbol{\Pi}_K^{k-1}\nabla(u-u_h) \leq \|\boldsymbol{\eta}\|_\infty\|u-u_h\|_{2,\Omega}^2 \leq C\gamma_h^2.$$

Thus, we obtain

$$|a(u-u_h,u-u_h)-\lambda b(u-u_h,u-u_h)|\leq C\gamma_h^2. \tag{4.7}$$

Next, to bound the third term, we consider $u_\pi\in L^2(\Omega)$ such that $u_\pi|_K\in\mathbb{P}_k(K)$ for all $K\in\mathcal{T}_h$ and Proposition 4.1 holds true. Hence, using the properties (3.8) and (3.9) of $a_{h,K}(\cdot,\cdot)$, we have

$$\begin{aligned}|a_h(u_h,u_h)-a(u_h,u_h)| &= \Big|\sum_{K\in\mathcal{T}_h}\Big\{a_{h,K}(u_h-u_\pi,u_h)-a_K(u_h-u_\pi,u_h)\Big\}\Big|\\ &\leq \sum_{K\in\mathcal{T}_h}(1+\alpha_2)a_K(u_h-u_\pi,u_h-u_\pi)\\ &\leq C\sum_{K\in\mathcal{T}_h}|u_h-u_\pi|_{2,K}^2.\end{aligned}$$

Then, adding and subtracting u, using the triangular inequality, Proposition 4.1 and (4.5), we get

$$|a_h(w_h,w_h)-a(w_h,w_h)|\leq C\big\{\gamma_h^2+h^{2\min\{s,k-1\}}\big\}. \tag{4.8}$$

On the other hand, the fourth term can be treated as follows:

$$\begin{aligned}b(u_h,u_h)-b_h(u_h,u_h) &= \sum_{K\in\mathcal{T}_h}\left\{\int_K\boldsymbol{\eta}\nabla u_h\cdot\nabla u_h-\int_K\boldsymbol{\eta}\boldsymbol{\Pi}_K^{k-1}\nabla u_h\cdot\boldsymbol{\Pi}_K^{k-1}\nabla u_h\right\}.\\ &= \sum_{K\in\mathcal{T}_h}\left\{\underbrace{\int_K\boldsymbol{\eta}\nabla u_h\cdot(\nabla u_h-\boldsymbol{\Pi}_K^{k-1}\nabla u_h)}_{E_1}+\underbrace{\int_K(\nabla u_h-\boldsymbol{\Pi}_K^{k-1}\nabla u_h)\cdot\boldsymbol{\eta}\boldsymbol{\Pi}_K^{k-1}\nabla u_h}_{E_2}\right\}.\end{aligned}$$

Now, we bound the terms E_1 and E_2. We start with E_1:

$$\begin{aligned}E_1 &= \int_K(\boldsymbol{\eta}\nabla u_h-\boldsymbol{\Pi}_K^{k-1}(\boldsymbol{\eta}\nabla u))\cdot(\nabla u_h-\boldsymbol{\Pi}_K^{k-1}\nabla u_h)\\ &= \int_K\Big(\boldsymbol{\eta}\nabla u_h-\boldsymbol{\eta}\nabla u+\boldsymbol{\eta}\nabla u-\boldsymbol{\Pi}_K^{k-1}(\boldsymbol{\eta}\nabla u)\Big)\cdot\Big(\nabla u_h-\nabla u+\nabla u-\boldsymbol{\Pi}_K^{k-1}\nabla u+\boldsymbol{\Pi}_K^{k-1}(\nabla u-\nabla u_h)\Big)\\ &\leq Ch^{2\min\{s,k-1\}},\end{aligned}$$

where in the last inequality we have used the triangular inequality, the approximation properties for $\boldsymbol{\Pi}_K^{k-1}$ (cf. Lemma 4.1), the additional regularity for the stress tensor $\boldsymbol{\eta}$ and the additional regularity for the eigenfunctions and finally (4.5) together with (4.4).

For the term E_2, we repeat the same arguments used to bound E_1, we obtain that

$$E_2\leq Ch^{2\min\{s,k-1\}}. \tag{4.9}$$

On the other hand, from Problem 2, Lemma 3.2 and the fact $\lambda_h^{(j)}\to\lambda$ when $h\to 0$, we have

$$|b_h(u_h,u_h)|=|\frac{1}{\lambda_h^{(j)}}a_h(u_h,u_h)|\geq\frac{\alpha}{|\lambda_h^{(j)}|}\|u_h\|_{2,\Omega}^2=\frac{\alpha}{|\lambda_h^{(j)}|}=C>0.$$

Thus, the proof follows from the above bound together with estimates (4.6)–(4.9). □

5. Numerical results

In this section, we report some numerical experiments to approximate the buckling coefficients considering different configurations of the problem, in order to confirm the theoretical results presented in this work for the cases $k=2$ and $k=3$. With this purpose, we have implemented in a MATLAB code the proposed discretization, following the arguments presented in [44].

To complete the construction of the discrete bilinear form, we have taken the symmetric form $s_K^D(\cdot,\cdot)$ as the euclidean scalar product associated to the degrees of freedom, properly scaled to satisfy (3.5) (see [11,23,33] for further details).

On the other hand, we have tested the method by using different families of meshes (see Figs. 1 and 8):

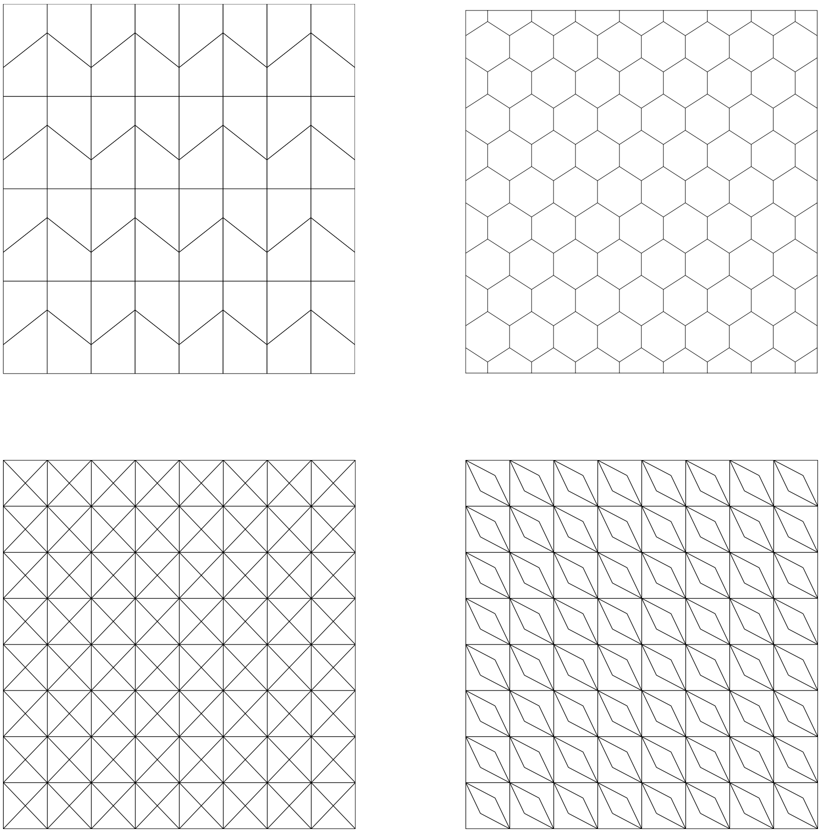

Fig. 1. Sample meshes: $\mathcal{T}_h^1$ (top left), $\mathcal{T}_h^2$ (top right), $\mathcal{T}_h^3$ (bottom left) and $\mathcal{T}_h^4$ (bottom right), for $N = 8$.

- $\mathcal{T}_h^1$: trapezoidal meshes which consist of partitions of the domain into $N \times N$ congruent trapezoids, all similar to the trapezoid with vertices $(0, 0)$, $(1/2, 0)$, $(1/2, 2/3)$ and $(0, 1/3)$;
- $\mathcal{T}_h^2$: hexagonal meshes;
- $\mathcal{T}_h^3$: triangular meshes;
- $\mathcal{T}_h^4$: distorted concave rhombic quadrilaterals;
- $\mathcal{T}_h^5$: Voronoi meshes which have been partitioned with N_P number of polygons.

We have used successive refinements of an initial mesh (see Fig. 1). The refinement parameter N used to label each mesh is the number of elements on each edge of the plate.

We have chosen four configurations for the computational domain Ω:

$$\Omega_S := (0, 1) \times (0, 1); \tag{5.10}$$

$$\Omega_L := (0, 1) \times (0, 1)\backslash[1/2, 1) \times [1/2, 1); \tag{5.11}$$

$$\Omega_C := \{(x, y) \in \mathbb{R}^2 : x^2 + y^2 < 1/4\}; \tag{5.12}$$

$$\Omega_H := (-5, 5) \times (-5, 5)\backslash\{(x, y) \in \mathbb{R}^2 : x^2 + y^2 < 9\}. \tag{5.13}$$

In order to compare our results for the buckling problem, we introduce a non-dimensional buckling coefficient, which is defined as:

$$\widehat{\lambda}_h^{(j)} := \frac{\lambda_h^{(j)} L}{\pi^2}, \tag{5.14}$$

where L is the plate side length.

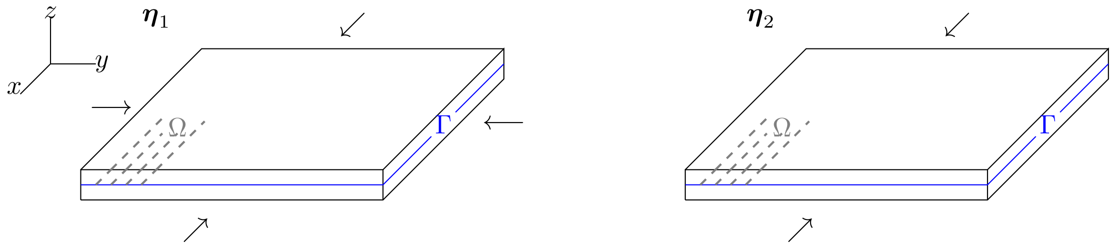

Fig. 2. η_1 (left) corresponds to a uniformly compressed plate (in the x, y directions) and η_2 (right) corresponds to a plate subjected to uniaxial compression (in the x direction).

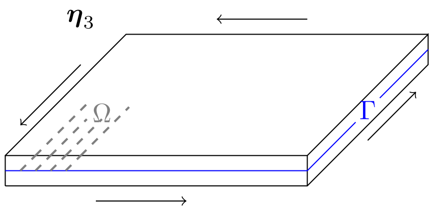

Fig. 3. η_3 corresponds to a plate subjected to shear load.

Moreover, we will consider different in-plane compressive stress $\boldsymbol{\eta}$. More precisely, we will compute the non-dimensional buckling coefficients using the following $\boldsymbol{\eta}$:

$$\boldsymbol{\eta}_1 := \begin{pmatrix} 1 & 0 \\ 0 & 1 \end{pmatrix}, \qquad \boldsymbol{\eta}_2 := \begin{pmatrix} 1 & 0 \\ 0 & 0 \end{pmatrix}, \qquad \boldsymbol{\eta}_3 := \begin{pmatrix} 0 & 1 \\ 1 & 0 \end{pmatrix}.$$

The physical meaning of the tensors $\boldsymbol{\eta}_1$, $\boldsymbol{\eta}_2$ and $\boldsymbol{\eta}_3$ is illustrated in Figs. 2 and 3, respectively.

5.1. Test 1: Clamped square plate

In this numerical test we compute the non-dimensional buckling coefficients (cf. (5.14)) for a uniformly compressed square plate Ω_S (cf. (5.10)). This corresponds to the stress field $\boldsymbol{\eta}_1$

We report in Table 1 the four lowest non-dimensional buckling coefficients computed with the virtual element method analyzed in this paper. The polynomial degrees are given by $k = 2, 3$ and with two different families of meshes and $N = 32, 64, 128$. The table includes orders of convergence as well as accurate values extrapolated by means of a least-squares fitting. In the last row of the table, we show the values obtained by extrapolating those computed with different method presented in [7]. (See Fig. 4.)

In this case, since Ω_S is convex, the problem have smooth eigenfunctions, as a consequence, when using degree k, the order of convergence is $2(k-1)$ as the theory predicts (cf. Theorem 4.4). Moreover, the results obtained by the two methods agree perfectly well.

In the next test we compute once again the non-dimensional buckling coefficients (in absolute value) of the same plate as in the previous example, subjected to a uniform shear load. This corresponds to the stress field $\boldsymbol{\eta}_3$.

In Table 2 we report the four lowest non-dimensional buckling coefficients (in absolute value) considering the stress field $\boldsymbol{\eta}_3$. Once again, the polynomial degrees are given by $k = 2, 3$ and with the mesh $\mathcal{T}_h^1$ and $N = 32, 64, 128$. The table includes orders of convergence as well as accurate values extrapolated by means of a least-squares fitting. In the last row of the table, we show the values obtained by extrapolating those computed with the method presented in [7].

Once again, it can be clearly observed from Table 2 that our method computes the scaled buckling coefficients (cf. (5.14)) with an optimal order of convergence and that the agreement with the method from [7] is excellent.

We show in Fig. 5 the buckling mode associated with the lowest scaled buckling coefficient.

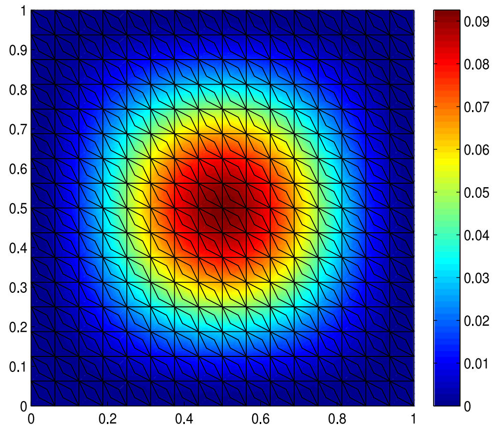

Fig. 4. Test 1. Buckling mode associated to the first non-dimensional buckling coefficient of a square clamped plate subjected to a plane stress tensor field $\boldsymbol{\eta}_1$.

Table 1
Test 1. Lowest non-dimensional buckling coefficients $\widehat{\lambda}_h^i$, $i = 1, 2, 3, 4$ of a clamped square plate subjected to a plane stress field $\boldsymbol{\eta}_1$.

Mesh	k	N	$\widehat{\lambda}_h^1$	$\widehat{\lambda}_h^2$	$\widehat{\lambda}_h^3$	$\widehat{\lambda}_h^4$
$\mathcal{T}_h^2$	2	32	5.2724	9.1716	9.2744	12.8252
		64	5.2952	9.2906	9.3174	12.9461
		128	5.3014	9.3229	9.3297	12.9786
		Order	1.86	1.88	1.80	1.89
		Extrap.	5.3038	9.3350	9.3347	12.9907
$\mathcal{T}_h^2$	3	32	5.3037	9.3345	9.3347	12.9918
		64	5.3036	9.3342	9.3342	12.9904
		128	5.3036	9.3342	9.3342	12.9904
		Order	3.95	3.95	3.94	3.93
		Extrap.	5.3036	9.3342	9.3342	12.9903
$\mathcal{T}_h^4$	2	32	5.3192	9.3581	9.3968	13.0934
		64	5.3075	9.3401	9.3498	13.0162
		128	5.3046	9.3356	9.3381	12.9968
		Order	2.00	2.00	2.00	1.99
		Extrap.	5.3036	9.3342	9.3341	12.9903
$\mathcal{T}_h^4$	3	32	5.3039	9.3348	9.3353	12.9939
		64	5.3036	9.3342	9.3342	12.9906
		128	5.3036	9.3342	9.3342	12.9904
		Order	3.94	3.93	3.93	3.91
		Extrap.	5.3036	9.3342	9.3342	12.9903
[7]			5.3037	9.3337	9.3337	12.9909

5.2. Test 2: Clamped L-shaped plate

In this numerical test, we consider an L-shaped domain: Ω_L (cf. (5.11)). We have used triangular and concave meshes as those shown in $\mathcal{T}_h^3$ and $\mathcal{T}_h^4$, respectively (see Fig. 1). Once again, the refinement parameter N is the number of elements on each edge.

Table 3 reports the four lowest non-dimensional buckling coefficient computed with the method analyzed in this paper with polynomial degree $k = 2$. We include in this table orders of convergence, as well as accurate values extrapolated by means of a least-squares fitting again. In the last row of the table, we show the values obtained by extrapolating those computed with different method presented in [7].

Table 2
Test 1. Lowest non-dimensional buckling coefficients (in absolute value) $\widehat{\lambda}_h^i$, $i = 1, 2, 3, 4$ of a clamped square plate subjected to a plane stress tensor field $\boldsymbol{\eta}_3$.

Mesh	k	N	$\widehat{\lambda}_h^1$	$\widehat{\lambda}_h^2$	$\widehat{\lambda}_h^3$	$\widehat{\lambda}_h^4$
		32	14.4988	16.6946	32.5980	34.5132
		64	14.6050	16.8607	33.1421	35.0854
$\mathcal{T}_h^1$	2	128	14.6327	16.9042	33.2905	35.2419
		Order	1.94	1.93	1.87	1.87
		Extrap.	14.6424	16.9197	33.3467	35.3009
		32	14.6459	16.9227	33.3660	35.3258
		64	14.6423	16.9191	33.3428	35.2975
$\mathcal{T}_h^1$	3	128	14.6420	16.9189	33.3413	35.2956
		Order	3.92	3.94	3.87	3.86
		Extrap.	14.6420	16.9188	33.3411	35.2955
[7]			14.6420	16.9195	33.3376	–

Table 3
Test 2. Four lowest non-dimensional buckling coefficient of a clamped L-shaped plate and subjected to a plane stress tensor field $\boldsymbol{\eta}_1$.

Mesh	k	N	$\widehat{\lambda}_{1h}$	$\widehat{\lambda}_{2h}$	$\widehat{\lambda}_{3h}$	$\widehat{\lambda}_{4h}$
		32	13.1749	15.0809	17.0798	19.9445
		64	13.0847	15.0234	17.0203	19.8758
$\mathcal{T}_h^3$	2	128	13.0495	15.0083	17.0042	19.8582
		Order	1.36	1.93	1.89	1.97
		Extrap.	13.0271	15.0029	16.9983	19.8522
		32	13.1949	15.1399	17.1801	20.1590
		64	13.0903	15.0388	17.0453	19.9297
$\mathcal{T}_h^4$	2	128	13.0511	15.0124	17.0105	19.8717
		Order	1.41	1.94	1.95	1.98
		Extrap.	13.0274	15.0031	16.9983	19.8519
		[7]	13.0290	15.0036	16.9949	–

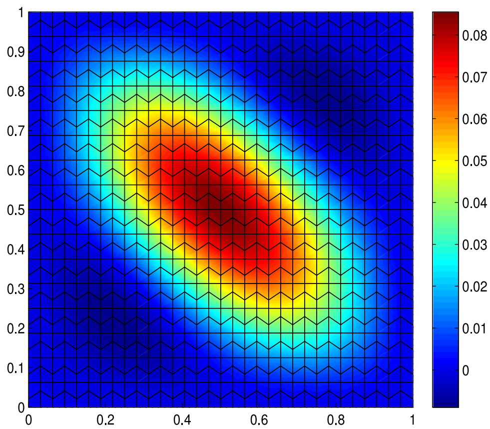

Fig. 5. Test 1. Buckling mode associated to the first non-dimensional buckling coefficient of a square plate subjected to a plane stress tensor field $\boldsymbol{\eta}_3$.

We observe that for the lowest non-dimensional buckling coefficient, the method converges with orders 1.36 and 1.41, for $\mathcal{T}_h^3$ and $\mathcal{T}_h^4$, respectively. We note that these orders of convergence are in accordance with the expected order which in this case is $2s = 1.089$ (see Theorem 4.4), because of the singularity of the solution (see [39]). For the other non-dimensional buckling coefficients, the method converges with larger orders.

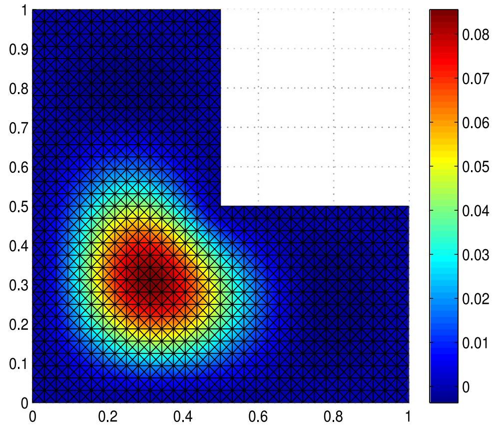

Fig. 6. Test 2. Buckling mode associated to the first non-dimensional buckling coefficient of a clamped L-shaped plate subjected to a plane stress tensor field $\boldsymbol{\eta}_1$.

We show in Fig. 6 the buckling mode associated with the lowest scaled buckling coefficient.

In this section, we consider an additional numerical test. We take the same configuration for the L-shaped domain as in the previous test: Ω_L. In this case, we solve the problem with polynomial degree $k = 3$ and we adopt a refinement with hanging nodes. In particular, the test is focused to validate the use of refined meshes as a tool to handle solutions with corner singularities. With this end, we have considered two families of meshes, namely: $\mathcal{T}_h^3$ and $\mathcal{T}_h^{3,\ell}$.

The mesh $\mathcal{T}_h^3$ consists in a sequence of uniform triangular meshes (see Fig. 1). The initial uniform mesh has $N = 16$ elements on each edge of the plate and the last one has $N = 64$ elements on each edge.

On the other hand, the mesh $\mathcal{T}_h^{3,\ell}$ is obtained by refining a patch around the re-entrant corner of Ω_L (cf. (5.11)), starting from an initial uniform triangular mesh $\mathcal{T}_h^{3,0}$ which corresponds to the first mesh of $\mathcal{T}_h^3$ (with $N = 16$). The procedure consists in to split each element which belongs to the region:

$$R_\ell := \left\{(x, y) \in \mathbb{R}^2 : |x - 1/2| \leq \frac{3}{N}2^{1-\ell} \quad \text{and} \quad |y - 1/2| \leq \frac{3}{N}2^{1-\ell}\right\} \cap \overline{\Omega}_L \qquad \ell = 1, 2, \ldots, \widehat{\ell},$$

into three quadrilaterals by connecting the barycenter of the element with the midpoint of each edge, where $\widehat{\ell}$ is the number of meshes to refine, with the convention that $\mathcal{T}_h^{3,0} := \mathcal{T}_h^3$ (the initial mesh with $N = 16$). Note that although this process is initiated with a triangular mesh, the successively created meshes will contain other kind of convex polygons as can be appreciated in Fig. 7.

In Table 4, we report the lowest non-dimensional buckling coefficient computed with the method analyzed in this paper with polynomial degree $k = 3$. Since the exact buckling coefficient is not known for this problem, we report a reference value obtained with the finite element method proposed in [7], in which a very fine triangular mesh was used. We compare the lowest non-dimensional buckling coefficient obtained by using uniform triangular meshes with those of $\mathcal{T}_h^{3,\ell}$. It is possible to observe that the reported errors are similar in the last row of each mesh in Table 4; however, the dofs in the case of corner-refined meshes are much less than the case of uniform meshes. As a consequence, we remark that the possibility of using more general meshes allow us easier refinements near edges and/or corners of the domain; therefore, the method has the potential of being competitive also in the presence of non-smooth solutions.

5.3. Test 3: Circular plate

In this test we solve the buckling problem on a circular plate Ω_C (cf. (5.12)). The domain Ω_C is partitioned using a sequence of polygonal meshes (Centroidal Voronoi tessellation) created with PolyMesher [45]. An example of the adopted meshes is shown in Fig. 8 with $N_P = 1024$.

We report in Table 5 the four lowest non-dimensional buckling coefficient ($L = 1$) for a circular clamped plate under uniform in-plane pressure. The table includes orders of convergences as well as accurate values extrapolated

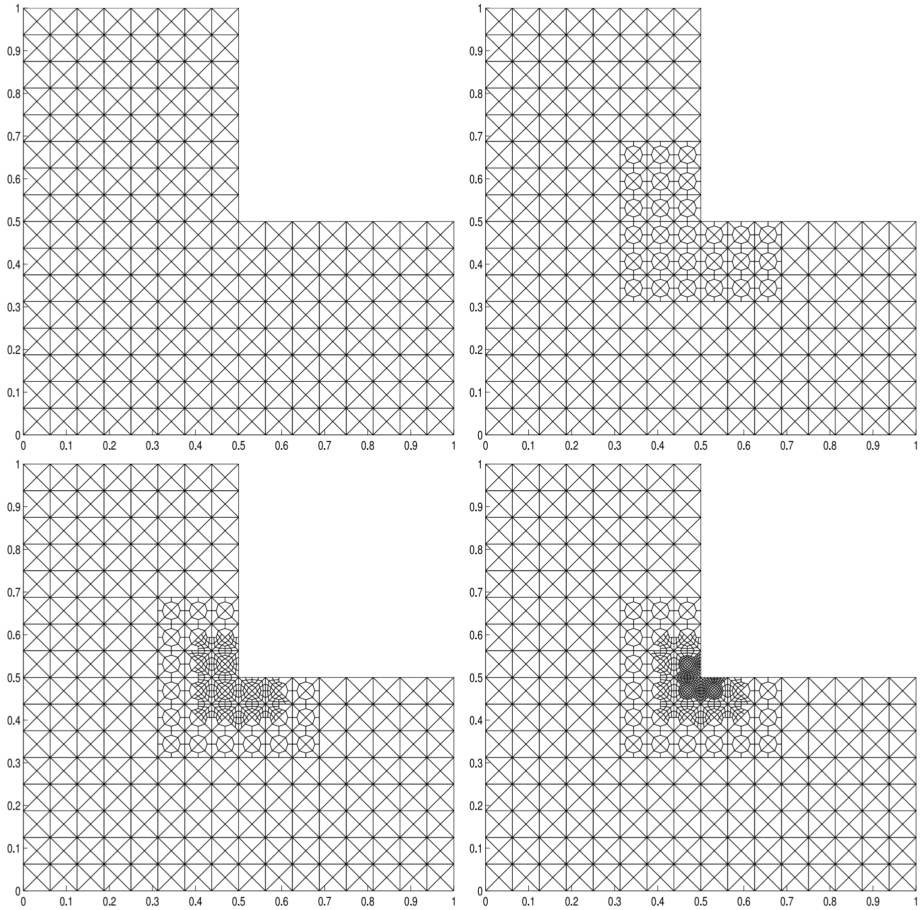

Fig. 7. Sample meshes: initial mesh $\mathcal{T}_h^{3,0}$ with $N = 16$ (top left), $\mathcal{T}_h^{3,1}$ (top right), $\mathcal{T}_h^{3,2}$ (bottom left) and $\mathcal{T}_h^{3,3}$ (bottom right).

Table 4
Test 2. Lowest non-dimensional buckling coefficient of a clamped L-shaped plate and subjected to a plane stress tensor field $\boldsymbol{\eta}_1$, by using uniform triangular meshes and polygonal meshes with hanging nodes.

Mesh	Dofs	$\widehat{\lambda}_{1h}$	Error
	2 179	13.1286430620	0.0996560949
$\mathcal{T}_h^3$	8 963	13.0711178812	0.0421309140
	36 355	13.0453680375	0.0163810704
ref.		13.0289869671	–
$\mathcal{T}_h^{3,0}$	2 179	13.1286430620	0.0996560949
$\mathcal{T}_h^{3,1}$	3 499	13.0869955611	0.0580085940
$\mathcal{T}_h^{3,2}$	5 005	13.0656232778	0.0366363107
$\mathcal{T}_h^{3,3}$	6 501	13.0533274578	0.0243404907
$\mathcal{T}_h^{3,4}$	7 947	13.0455813044	0.0165943372
ref.		13.0289869671	–

Table 5
Test 3. Lowest non-dimensional buckling coefficients $\widehat{\lambda}_h^i$, $i = 1, 2, 3, 4$ of a circular clamped plate subjected to a plane stress field $\boldsymbol{\eta}_1$.

Mesh	k	N_P	$\widehat{\lambda}_h^1$	$\widehat{\lambda}_h^2$	$\widehat{\lambda}_h^3$	$\widehat{\lambda}_h^4$
		1 024	5.8962	10.5171	10.5249	16.1264
		4 096	5.9365	10.6455	10.6469	16.3993
$\mathcal{T}_h^5$	2	16 384	5.9469	10.6783	10.6783	16.4720
		Order	1.95	1.97	1.96	1.91
		Extrap.	5.9506	10.6895	10.6891	16.4983
		1 024	5.9494	10.6868	10.6872	16.4931
		4 096	5.9503	10.6891	10.6891	16.4974
$\mathcal{T}_h^5$	3	16 384	5.9503	10.6891	10.6891	16.4974
		Order	4.00	4.00	4.00	4.00
		Extrap.	5.9503	10.6891	10.6891	16.4976
[46]			5.9503	–	–	–

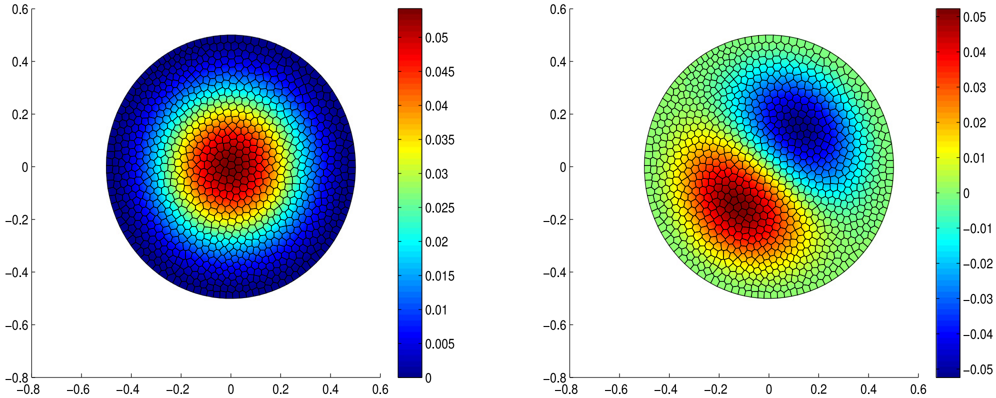

Fig. 8. Test 3. Buckling modes associated to the lowest non-dimensional buckling coefficients $\widehat{\lambda}_h^1$ (left) and $\widehat{\lambda}_h^2$ (right) of a circular clamped plate under uniform in-plane pressure $\boldsymbol{\eta}_1$.

by means of a least-squares fitting. We compare the performance of the proposed method with those presented in [46] for Reissner–Mindlin plates with very small thickness. It is well known that when the thickness goes to zero the solution of the Reissner–Mindlin model converges to an identical Kirchhoff–Love solution.

It can be clearly seen from Table 5 that our method computes the scaled buckling coefficients with an optimal order of convergence. Moreover, an excellent agreement with the result presented in [46] can be clearly appreciated.

Fig. 8 shows the buckling modes corresponding to the two lowest non-dimensional buckling coefficient of a circular clamped plate.

5.4. Test 4: Simply supported-free square plate

In this test we have computed the non-dimensional buckling coefficient of a simply supported-free square plate (see Remark 2.2), subjected to linearly varying in-plane load in one direction (x direction). This corresponds to a plane stress field given by

$$\widetilde{\boldsymbol{\eta}}_2 := \begin{pmatrix} 1-\alpha\frac{y}{L} & 0 \\ 0 & 0 \end{pmatrix}, \tag{5.15}$$

with values of α in $\{0, 2/3, 1, 4/3, 2\}$. We observe that for $\alpha = 0$, we obtain the plane stress tensor field $\boldsymbol{\eta}_2$.

We take an square plate Ω_S which has two simply supported edges and two free edges.

We report in Table 6 the lowest non-dimensional buckling coefficient for different values of α. The polynomial degrees are given by $k = 2, 3$ and the family of meshes $\mathcal{T}_h^2$ with $N = 32, 64, 128$. The table includes computed

Table 6
Test 4. Non-dimensional buckling coefficient $\widehat{\lambda}_{1h}$ for different values of α of a square plate with mixed boundary conditions and subjected to linearly varying in-plane load in one direction $\widetilde{\boldsymbol{\eta}}_2$.

Mesh	k	N	$\alpha=0$	$\alpha=2/3$	$\alpha=1$	$\alpha=4/3$	$\alpha=2$
		32	0.9984	1.4474	1.7763	2.1687	3.0676
		64	0.9996	1.4490	1.7782	2.1709	3.0702
$\mathcal{T}_h^2$	2	128	0.9999	1.4495	1.7787	2.1715	3.0710
		Order	1.91	1.90	1.90	1.88	1.85
		Extrap.	1.0000	1.4496	1.7789	2.1717	3.0713
		32	1.0000	1.4496	1.7789	2.1717	3.0712
		64	1.0000	1.4496	1.7789	2.1717	3.0712
$\mathcal{T}_h^2$	3	128	1.0000	1.4496	1.7789	2.1717	3.0712
		Order	4.00	4.00	4.00	4.00	4.00
		Extrap.	1.0000	1.4496	1.7789	2.1717	3.0712

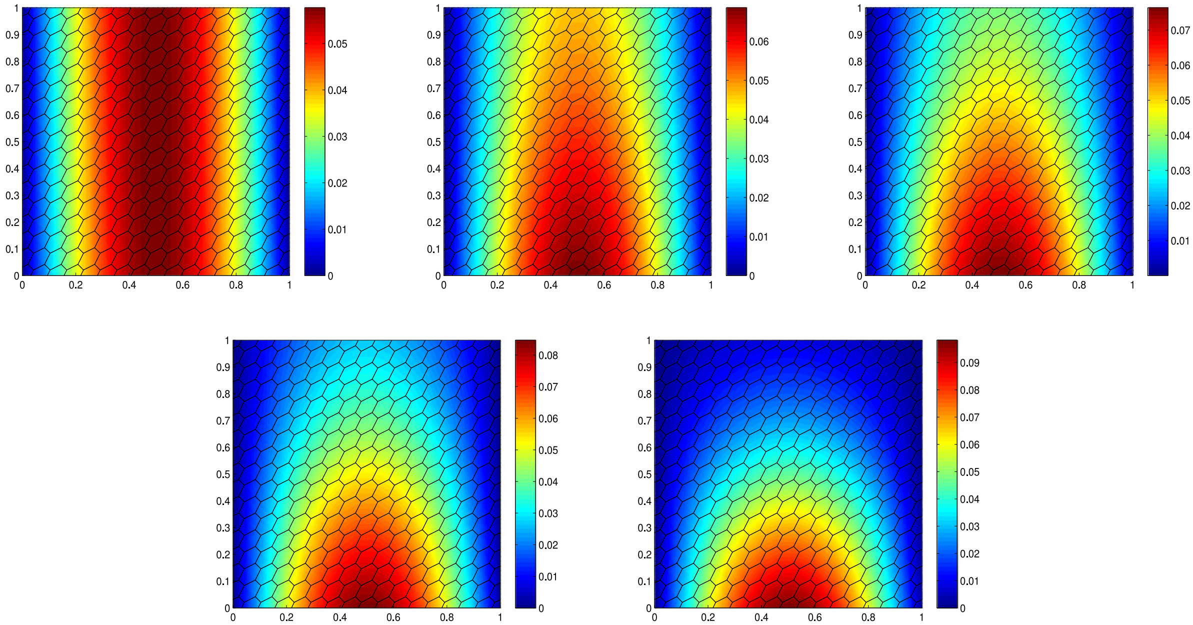

Fig. 9. Test 4. Buckling modes associated to the lowest non-dimensional buckling coefficient $\widehat{\lambda}_h^1$ of a square plate with mixed boundary conditions and subjected to linearly varying in-plane load in one direction $\widetilde{\boldsymbol{\eta}}_2$ (cf. (5.15)): $\alpha=0$ (top left), $\alpha=2/3$ (top middle), $\alpha=1$ (top right), $\alpha=4/3$ (bottom left), $\alpha=2$ (bottom right).

orders of convergence and extrapolated more accurate values of each eigenvalue obtained by means of a least-squares fitting.

It can be clearly observed from Table 6 that the proposed virtual scheme computes the scaled buckling coefficient (cf. (5.14)) with an optimal order of convergence for all the values of α.

Finally, we show in Fig. 9 the buckling mode associated with the lowest scaled buckling coefficient for different values of the parameter α.

5.5. *Test 5: A square plate with a hole subjected to different in-plane loads*

In this final numerical test, we compute the buckling coefficients and modes of a clamped (CCCC) and a simply supported (SSSS) square plate with a hole (free). We have taken Ω_H (cf. (5.13), where all of the lengths are measured

Table 7
Test 5: Lowest non-dimensional buckling load intensity factor k.

N_P	CCCC			SSSS		
	η_1	η_2	η_3	η_1	η_2	η_3
400	6.594	11.848	24.622	1.464	2.849	12.578
1600	6.594	11.856	24.696	1.465	2.851	12.602
6400	6.593	11.858	24.713	1.465	2.852	12.605

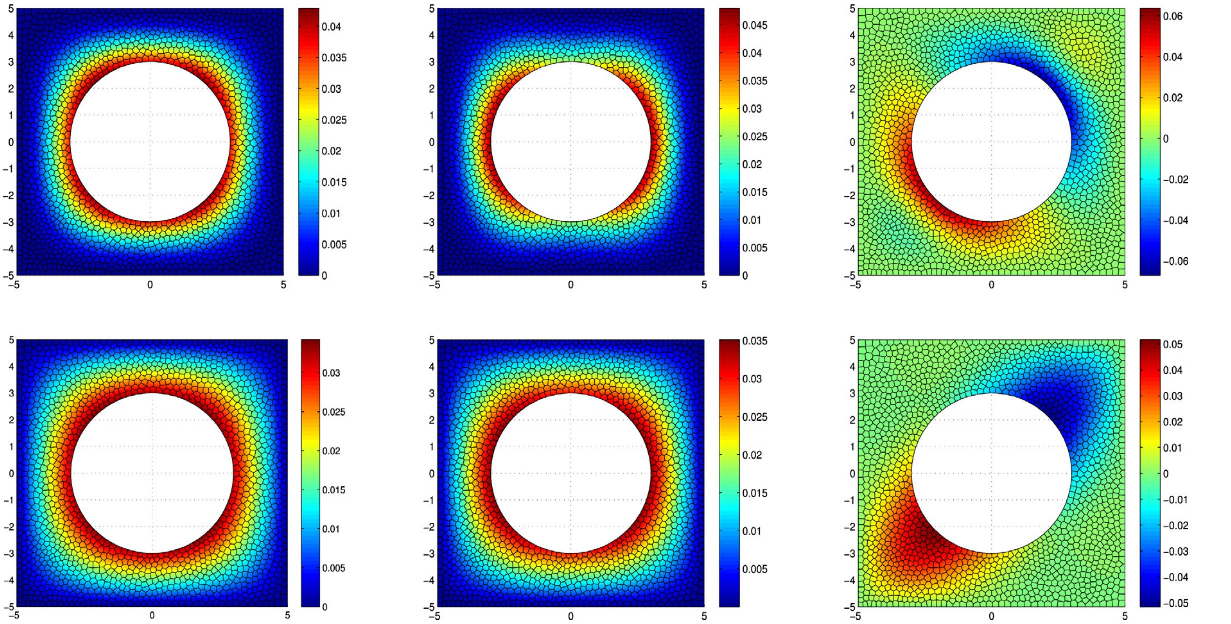

Fig. 10. Test 5. Buckling modes associated to the lowest non-dimensional buckling coefficient k of a square clamped plate with a hole and subjected to a plane stress tensor fields $\boldsymbol{\eta}_1$ (top left), $\boldsymbol{\eta}_2$ (top middle), and $\boldsymbol{\eta}_3$ (top right). Buckling modes associated to the lowest non-dimensional buckling coefficient k of a square simply supported plate with a hole and subjected to a plane stress tensor fields $\boldsymbol{\eta}_1$ (bottom left), $\boldsymbol{\eta}_2$ (bottom middle), and $\boldsymbol{\eta}_3$ (bottom right).

in meters m). In this case, instead of (2.1), we have solved the following eigenvalue problem:

$$B_D \Delta^2 u = -\lambda \operatorname{div}(\boldsymbol{\eta}\nabla u) \quad \text{in } \Omega,$$

where $B_D := \frac{Et^3}{12(1-\nu^2)}$ is the bending rigidity with the material parameters $E = 200 \times 10^9 \frac{N}{m^2}$, $t = 1$ and $\nu = 0.3$.

In addition, the results are presented in terms of the following non-dimensional buckling load intensity factor defined as $k := \frac{L^2 \lambda_h^{(1)}}{\pi^2 B_D}$.

The domain Ω_H is partitioned using a sequence of Voronoi polygonal meshes created with PolyMesher [45], each mesh with N_P polygons. An example of the adopted meshes is shown in Fig. 10.

We report in Table 7 the lowest non-dimensional buckling load intensity factor k for three different in-plane load cases; namely, $\boldsymbol{\eta}_1$, $\boldsymbol{\eta}_2$ and $\boldsymbol{\eta}_3$.

Finally, we show in Fig. 10 the buckling modes associated with the lowest non-dimensional buckling load intensity factor k for a clamped and a simply supported square plate with a hole, respectively.

Acknowledgments

The First author was partially supported by CONICYT-Chile through FONDECYT project 1180913 and by project AFB170001 of the PIA Program: Concurso Apoyo a Centros Científicos y Tecnológicos de Excelencia con Financiamiento Basal. The second author was partially supported by a CONICYT-Chile fellowship.

References

[1] S.C. Brenner, P. Monk, J. Sun, C^0 interior penalty Galerkin method for biharmonic eigenvalue problems, in: Spectral and High Order Methods for Partial Differential Equations, in: Lect. Notes Comput. Sci. Eng., vol. 106, 2015, pp. 3–15.

[2] J. Cao, Z. Wang, W. Cao, L. Chen, A mixed Legendre–Galerkin spectral method for the buckling problem of simply supported Kirchhoff plates, Bound. Value Probl. 34 (2017) 1–12.

[3] Ö. Civalek, A. Korkmazb, Ç. Demir, Discrete singular convolution approach for buckling analysis of rectangular Kirchhoff plates subjected to compressive loads on two-opposite edges, Adv. Eng. Softw. 41 (2010) 557–560.

[4] P. Hansbo, M.G. Larson, A posteriori error estimates for continuous/discontinuous Galerkin approximations of the Kirchhoff–Love buckling problem, Comput. Mech. 56 (2015) 815–827.

[5] K. Ishihara, On the mixed finite element approximation for the buckling of plates, Numer. Math. 33 (1979) 195–210.

[6] F. Millar, D. Mora, A finite element method for the buckling problem of simply supported Kirchhoff plates, J. Comput. Appl. Math. 286 (2015) 68–78.

[7] D. Mora, R. Rodríguez, A piecewise linear finite element method for the buckling and the vibration problems of thin plates, Math. Comp. 78 (2009) 1891–1917.

[8] R. Rannacher, Nonconforming finite element methods for eigenvalue problems in linear plate theory, Numer. Math. 33 (1979) 23–42.

[9] L. Beirão da Veiga, F. Brezzi, A. Cangiani, G. Manzini, L.D. Marini, A. Russo, Basic principles of virtual element methods, Math. Models Methods Appl. Sci. 23 (2013) 199–214.

[10] P.F. Antonietti, L. Beirão da Veiga, D. Mora, M. Verani, A stream virtual element formulation of the Stokes problem on polygonal meshes, SIAM J. Numer. Anal. 52 (2014) 386–404.

[11] P.F. Antonietti, L. Beirão da Veiga, S. Scacchi, M. Verani, A C^1 virtual element method for the Cahn–Hilliard equation with polygonal meshes, SIAM J. Numer. Anal. 54 (2016) 36–56.

[12] E. Artioli, S. de Miranda, C. Lovadina, L. Patruno, A family of virtual element methods for plane elasticity problems based on the Hellinger–Reissner principle, Comput. Methods Appl. Mech. Engrg. 340 (2018) 978–999.

[13] L. Beirão da Veiga, F. Brezzi, F. Dassi, L.D. Marini, A. Russo, Virtual element approximation of 2D magnetostatic problems, Comput. Methods Appl. Mech. Engrg. 327 (2017) 173–195.

[14] L. Beirão da Veiga, F. Brezzi, F. Dassi, L.D. Marini, A. Russo, Lowest order virtual element approximation of magnetostatic problems, Comput. Methods Appl. Mech. Engrg. 332 (2018) 343–362.

[15] L. Beirão da Veiga, F. Brezzi, L.D. Marini, Virtual elements for linear elasticity problems, SIAM J. Numer. Anal. 51 (2013) 794–812.

[16] L. Beirão da Veiga, C. Lovadina, D. Mora, A virtual element method for elastic and inelastic problems on polytope meshes, Comput. Methods Appl. Mech. Engrg. 295 (2015) 327–346.

[17] L. Beirão da Veiga, C. Lovadina, G. Vacca, Divergence free virtual elements for the Stokes problem on polygonal meshes, ESAIM Math. Model. Numer. Anal. 51 (2017) 509–535.

[18] M.F. Benedetto, S. Berrone, A. Borio, S. Pieraccini, S. Scialò, Order preserving SUPG stabilization for the virtual element formulation of advection–diffusion problems, Comput. Methods Appl. Mech. Engrg. 311 (2016) 18–40.

[19] S.C. Brenner, Q. Guan, L.-Y. Sung, Some estimates for virtual element methods, Comput. Methods Appl. Math. 17 (2017) 553–574.

[20] E. Cáceres, G.N. Gatica, A mixed virtual element method for the pseudostress-velocity formulation of the Stokes problem, IMA J. Numer. Anal. 37 (2017) 296–331.

[21] E. Cáceres, G.N. Gatica, F. Sequeira, A mixed virtual element method for the Brinkman problem, Math. Models Methods Appl. Sci. 27 (2017) 707–743.

[22] A. Cangiani, G. Manzini, O.J. Sutton, Conforming and nonconforming virtual element methods for elliptic problems, IMA J. Numer. Anal. 37 (2017) 1317–1354.

[23] C. Chinosi, L.D. Marini, Virtual element method for fourth order problems: L^2-estimates, Comput. Math. Appl. 72 (2016) 1959–1967.

[24] L. Mascotto, I. Perugia, A. Pichler, Non-conforming harmonic virtual element method: h- and p- versions, J. Sci. Comput. 77 (2018) 1874–1908.

[25] I. Perugia, P. Pietra, A. Russo, A plane wave virtual element method for the Helmholtz problem, ESAIM Math. Model. Numer. Anal. 50 (2016) 783–808.

[26] G. Vacca, An H^1-conforming virtual element for Darcy and Brinkman equations, Math. Models Methods Appl. Sci. 28 (2018) 159–194.

[27] P. Wriggers, W.T. Rust, B.D. Reddy, A virtual element method for contact, Comput. Mech. 58 (2016) 1039–1050.

[28] L. Beirão da Veiga, D. Mora, G. Rivera, R. Rodríguez, A virtual element method for the acoustic vibration problem, Numer. Math. 136 (2017) 725–763.

[29] F. Gardini, G. Manzini, G. Vacca, The nonconforming virtual element method for eigenvalue problems, ESAIM Math. Model. Numer. Anal. 53 (2019) 749–774.

[30] F. Gardini, G. Vacca, Virtual element method for second-order elliptic eigenvalue problems, IMA J. Numer. Anal. 38 (2018) 2026–2054.

[31] D. Mora, G. Rivera, A priori and a posteriori error estimates for a virtual element spectral analysis for the elasticity equations, IMA J. Numer. Anal. (2019) DOI: https://doi.org/10.1093/imanum/dry063.

[32] D. Mora, G. Rivera, R. Rodríguez, A virtual element method for the Steklov eigenvalue problem, Math. Models Methods Appl. Sci. 25 (2015) 1421–1445.

[33] D. Mora, G. Rivera, I. Velásquez, A virtual element method for the vibration problem of Kirchhoff plates, ESAIM Math. Model. Numer. Anal. 52 (2018) 1437–1456.

[34] D. Mora, I. Velásquez, A virtual element method for the transmission eigenvalue problem, Math. Models Methods Appl. Sci. 28 (2018) 2803–2831.

[35] F. Brezzi, L.D. Marini, Virtual elements for plate bending problems, Comput. Methods Appl. Mech. Engrg. 253 (2013) 455–462.

[36] P.G. Ciarlet, The Finite Element Method for Elliptic Problems, SIAM, 2002.
[37] I. Babuška, J. Osborn, in: P.G. Ciarlet and J.L. Lions (Ed.), Eigenvalue problems, in Handbook of Numerical Analysis, Vol. II, North-Holland, Amsterdam, 1991, pp. 641–787.
[38] S.P. Timoshenko, J.M. Gere, Theory of Elastic Stability, McGraw-Hill, New York, 1961.
[39] P. Grisvard, Elliptic Problems in Non-Smooth Domains, Pitman, Boston, 1985.
[40] B. Ahmad, A. Alsaedi, F. Brezzi, L.D. Marini, A. Russo, Equivalent projectors for virtual element methods, Comput. Math. Appl. 66 (2013) 376–391.
[41] V. Girault, P.A. Raviart, Finite Element Methods for Navier–Stokes Equations, Springer-Verlag, Berlin, 1986.
[42] S.C. Brenner, R.L. Scott, The Mathematical Theory of Finite Element Methods, Springer, New York, 2008.
[43] L. Beirão da Veiga, D. Mora, G. Rivera, Virtual elements for a shear-deflection formulation of Reissner–Mindlin plates, Math. Comp. 88 (2019) 149–178.
[44] L. Beirão da Veiga, F. Brezzi, L.D. Marini, A. Russo, The hitchhiker's guide to the virtual element method, Math. Models Methods Appl. Sci. 24 (2014) 1541–1573.
[45] C. Talischi, G.H. Paulino, A. Pereira, I.F.M. Menezes, PolyMesher: a general-purpose mesh generator for poygonal elements written in Matlab, Struct. Multidiscip. Optim. 45 (2012) 309–328.
[46] C.M. Wang, A. Tun Myint, A plastic buckling analysis of thick plates using p-Ritz method, Int. J. Solids Struct. 44 (2007) 6239–6255.